Geometrical frustration and competing orders in the dipolar trimerized triangular lattice

Kevin Hofhuis, Charlotte F. Petersen, Michael Saccone, Scott Dhuey, Armin Kleibert, Sebastiaan van Dijken, and Alan Farhan

Phys. Rev. B **104**, 014409 — Published 8 July 2021

DOI: 10.1103/PhysRevB.104.014409

Geometrical frustration and competing orders in the dipolar trimerized triangular lattice

Kevin Hofhuis,[1, 2] Charlotte F. Petersen,[3] Michael Saccone,[4, 5] Scott Dhuey,[6]
Armin Kleibert,[7] Sebastiaan van Dijken,[8] and Alan Farhan[2, 8, *]
[1] *Laboratory for Mesoscopic Systems, Department of Materials, ETH Zurich, 8093 Zurich, Switzerland*
[2] *Laboratory for Multiscale Materials Experiments,*
Paul Scherrer Institute, 5232 Villigen PSI, Switzerland
[3] *Australian Institute for Bioengineering and Nanotechnology,*
The University of Queensland, Brisbane, Queensland 4072, Australia
[4] *Center for Nonlinear Studies, Los Alamos National Laboratory, Los Alamos, New Mexico 87545, USA*
[5] *Theoretical Division (T4), Los Alamos National Laboratory, Los Alamos, New Mexico 87545, USA*
[6] *Molecular Foundry, Lawrence Berkeley National Laboratory, One Cyclotron Road, CA 94720, USA*
[7] *Swiss Light Source, Paul Scherrer Institute, 5232 Villigen PSI, Switzerland*
[8] *Department of Applied Physics, Aalto University School of Science, P.O. Box 15100, FI-00076 Aalto, Finland*

(Dated: June 10, 2021)

We introduce and explore low-energy configurations in two-dimensional arrays consisting of Ising-type dipolar coupled nanomagnets lithographically defined onto three-nanomagnet vertices arranged in a triangular coordination. Thus, the system is dubbed the trimerized triangular lattice. Employing synchrotron-based photoemission electron microscopy (PEEM), we perform temperature-dependent magnetic imaging of moment configurations. These states are then characterized in terms of spin correlations and magnetic structure factors. The results reveal a competition between ferromagnetic and vortex dominated orders, which can be controlled by varying the relevant lattice parameter and the corresponding competing interactions.

I. INTRODUCTION

Artificial spin ices are nanomagnetic systems consisting of monodomain Ising-type nanomagnets that are lithographically defined onto two- and three-dimensional lattices[1–21]. While initially introduced as two-dimensional artificial analogues to pyrochlore spin ice[22], they have increasingly become a popular playground to directly visualize the consequences of geometrical spin frustration using appropriate imagine techniques[23], particularly after the realization of thermally-induced moment fluctuations at experimentally accessible temperatures[7]. Studies range from real-time observations of thermal fluctuations in classical artificial kagome[7,14] and square spin ice[24,25], the realization of reduced and elevated effective dimensionality[10,26] to the first attempts in achieving artificial Ising spin glasses[27]. Interest in these systems was spurred further by observations of field- and temperature-driven dynamics of emergent magnetic monopoles in macroscopically degenerate artificial square ice structures[13,19], field-induced phase coexistence in a quadrupolar artificial spin ice[28], and extensive studies on the dynamic response of artificial spin ice systems[29–33] and tunable hybrid systems[34,35]. In addition, colloidal and macroscopic artificial spin ice systems have also gained increasing popularity[36–40].

Among all nanomagnetic systems mentioned above, artificial kagome spin ice, with its strict ice-rule obedience[7,14], extensive degeneracy, short-range order and non-trivial ground state[14,41–43], has attracted a considerable amount of research interest over the past years. The ice-rule obeying three-nanomagnet kagome vertices or trimers also served as basic building blocks for various artificial frustrated systems with mixed coordination numbers[8,11,17,44], where these vertices are combined either with the well known four-nanomagnet vertices from artificial square ice[2,24] or the six-nanomagnet vertices appearing in artificial triangular spin ice patterns[45,46]. Artificial triangular spin ice, has been investigated both in its nanomagnetic form[45,46] and colloidal version[38]. In both cases, it has been shown to lack strong frustration or extensive ground state degeneracy. As a result, it is expected to access long-range order once thermally activated, similar to two-dimensional artificial square ice[24,47]. This raises the question whether a strategy can be implemented, to re-organize the triangular lattice, so that it would exhibit a higher degree of frustration and competing orderings.

In the present work, we address this question by introducing a nanomagnet geometry that shares elements of both artificial kagome- and triangular spin ice systems. We dub it the trimerized triangular lattice. To form this lattice, three-nanomagnet vertices or trimers (see Fig. 1a) are arranged periodically with a 60° coordination, resulting in an array as depicted in Fig. 1a and Fig. 1b. A unique situation emerges in this geometry: First, dipolar interaction between the moments at the trimers (see J_1 in Fig. 1a and α and β in Fig. 1b) try to enforce ice-rule domination (two-in/one-out or one-in/two-out). Second, interactions α and γ (see Fig. 1b and J_2 in Fig. 1a) prefer the formation of clockwise and anti-clockwise vortices. These two ordering preferences are not fully compatible with one another. The formation of vortices leads to ice-rule violations, whereas an ice-rule dictated structure destroys the vortex configurations. (see illustrations in Fig. 1c and Fig. 1d-f). The other nearest-neighbor inter-

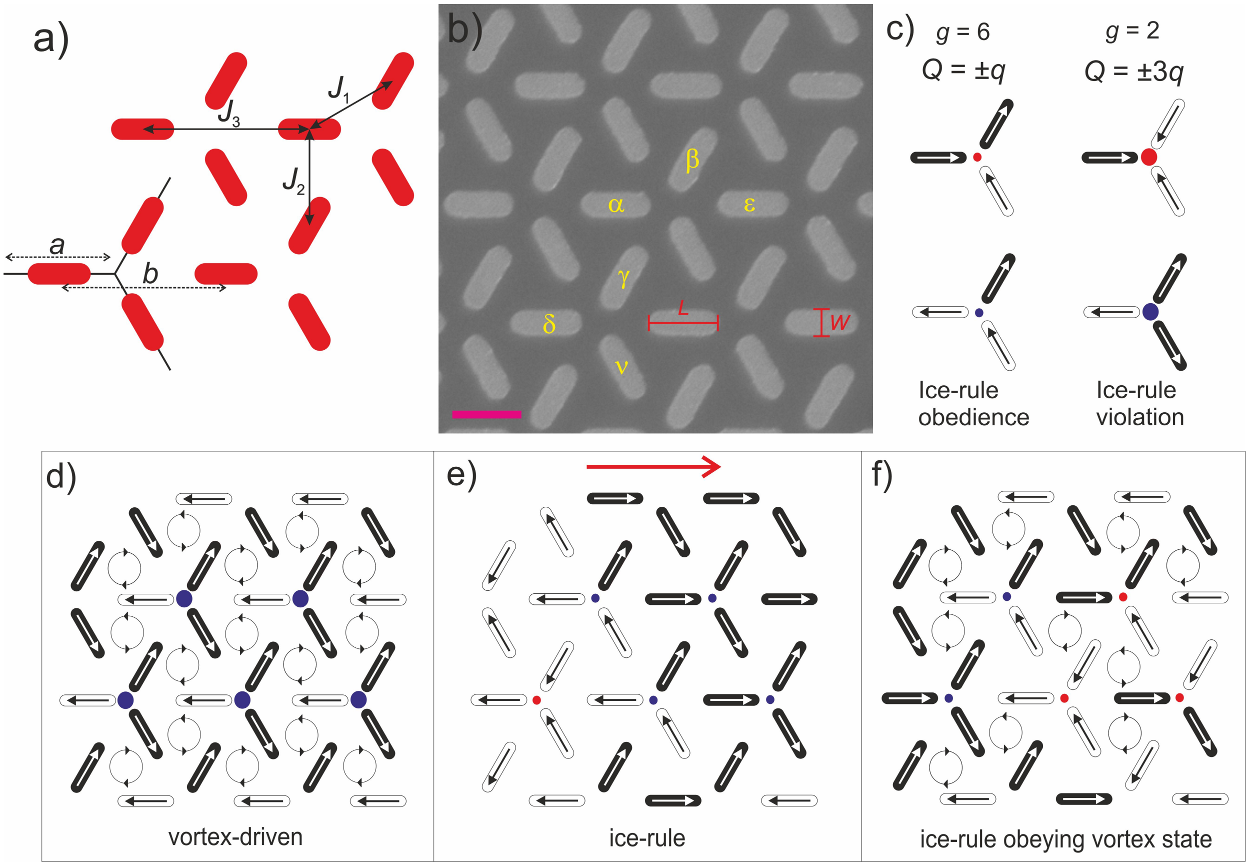

FIG. 1. (a) Trimerized triangular lattice. Dipolar-coupled Ising-type nanomagnets (red stadium-shapes) occupy the sites of kagome three-nanomagnet vertices (or trimers) with lattice parameter $a = 450$ nm and a vertex-to-vertex separation parameter $b = 500$-800 nm. (b) Scanning electron microscopy (SEM) image of one of the trimerized triangular lattice ($b = 615$ nm) consisting of Ising-type nanomagnets with lengths $L = 300$ nm and widths $W = 100$ nm. (c) Possible spin configuration at the three-nanomagnet vertices. Left: Ice-rule (two-in/one-out or one-in/two-out) obeying configurations exhibit a six-fold degeneracy ($g = 6$) and a vertex charge $Q = \pm q$. Right: Ice-rule violating (three-in or three-out) configurations exhibit a two-fold degeneracy ($g = 2$) and a vertex charge $Q = \pm 3q$, highlighted by a larger colored circle at the centre of each vertex. (d)-(f) Ordering competition in the trimerized triangular lattice. (d) Schematic drawing of a vortex-driven moment configuration consisting of 100% clockwise and anti-clockwise vortices, which can only be fulfilled by violating the ice-rule at each three-nanomagnet vertex. (e) Ferromagnetic ice-rule dominated state, which does not necessarily support the formation of vortices. (f) A configuration that strictly obeys the ice-rule, but attempts at maximizing vortex formations can only be constructed with clockwise- and anti-clockwise vortices forming at around 66% of all triangles. The dark and bright coloring of nanomagnets in (d)-(f) corresponds to the contrast observed in XMCD images. Magnetic moments pointing towards the incoming X-rays (red arrow in (e)) will appear dark, while moments with a non-zero component opposing the incoming X-rays will appear bright.

action, J_3, couples collinear nanomagnets from vertex to vertex and supports the formation of ferromagnetic-type moment configurations. It is the interplay of J_1, J_2 and J_3 that will dictate ordering preferences, as the lattice parameter b is varied.

II. METHODS

A. Sample Fabrication and Magnetic Imaging

Dipolar trimerized triangular lattice structures are fabricated using a lift-off assisted electron-beam lithography process. This process includes the following steps: A 1×1 cm^2 silicon (100) substrate is first spin coated with a 70-nm-thick layer of polymethylmethacrylate (PMMA) resist. This is followed by electron-beam exposure, where patterns of interest are then defined onto the substrate using a VISTEC VB300 electron-beam writer. Next, a 2.7 nm thick ferromagnetic permalloy ($Ni_{80}Fe_{20}$) film is thermally deposited at a base pressure of 2×10^{-7} torr. This is followed by lift-off in acetone at a temperature of 50° C, where all unwanted magnetic material is removed. This process results in dipolar trimerized triangular lattices consisting of nanomagnets with lengths $L = 300$ nm, widths $W = 100$ nm and thickness $d = 2.7$ nm (see example in Fig. 1b). Structures with lattice parameter $b = 500$ nm, 545 nm, 600 nm, 615 nm, 625 nm, 700 nm, and 800 nm are generated. Each array covered an area of 60×60 μm^2.

Magnetic imaging was performed using the photoemission electron microscopy (PEEM) endstation at the SIM beamline of the Swiss Light Source[48]. Dealing with ferromagnetic permalloy nanostructures, we employ X-ray magnetic circular dichroism (XMCD) at the Fe L3 edge[49].

B. Micromagnetic Simulations

The strengths of the pair-wise interactions (J_1, J_2 and J_3) for the dipolar trimerized triangular lattice are simulated using the micromagnetic package MuMax3[50] and equation $E = J_{\mathrm{ij}}\sigma_{\mathrm{i}}\sigma_{\mathrm{j}} + E_0$, where J_{ij} is the pair-wise interaction strength, $\sigma_{\mathrm{ij}} = \pm 1$ is the mesoscopic Ising spin state, and E_0 is the self-energy of the system without any interactions. Simulations are performed using bulk material parameters for Permalloy nanomagnets with a lateral dimension of 300 x 100 nm^2 (L x W): a saturation magnetization M_{sat} of 790 kA/m, an exchange stiffness constant A_{ex} of 13 pJ/m, and zero magnetocrystalline anisotropy. The cell size is 2 x 2 x 2.5 nm^3, and the lattice parameter a is 450 nm, while the parameter b is varied from 400 to 800 nm in steps of 10 nm. These simulations reveal that competing interactions J_1 and J_2 equalize around b = 542 nm (see Fig. 2), marking the point where we expect the highest degree of frustration and ordering competition. As b increases, J_2 and J_3 continue to decrease, while J_1 remains constant (see Fig. 2) and is expected to dominate at higher values of b. In other words, as J_1 domination sets in, we expect configurations that adhere to ice-rule (see Fig. 1c) constraints, but where the weakened influence of J_2 and J_3 will still contribute to ordering preferences.

III. RESULTS

A. Thermal annealing and low-energy states

Following sample fabrication, the samples were placed in a vacuum at room temperature for several weeks. The chosen nanomagnet thickness of 2.7 nm and lateral dimensions (L = 300 nm and W = 100 nm) are chosen, so that thermally-driven moment reorientation within the patterned nanomagnets at the timescale of a few seconds starts at blocking temperatures T_B below 200 K[11,17,51]. Therefore, the room temperature waiting period ensures that structures have enough time to relax towards their low energy configurations[15,17]. Following this annealing procedure, the sample is transferred into the PEEM and cooled down to 90 K (below T_B), after which XMCD magnetic contrast maps are recorded (see Fig. 3a-d). For statistics, this process was repeated up to three times on four different arrays of the same lattice parameter. For small lattice parameters b = 500 nm, we see long-range ordered configurations dominated by clockwise and anticlockwise vortices (see example in Fig. 3a and illustration in Fig. 1d). This is the same ground state predicted for the so-called artificial triangular spin ice[45]. As predicted by the aforementioned micromagnetic simulations, the annealed moment configurations achieved in the structure with b = 545 nm reveals a high degree of ordering competition, as we see small clusters of both ice-rule obeying configurations and vortex-dominated formations (see Fig. 3b), without any particular configuration being able to dominate. This indicates that competing interactions are equalized, and maximum frustration is achieved. As b is increased further, we start to see a transition towards configurations consisting of larger ferromagnetic-type domains (see an example of a domain highlighted with a dashed magenta frame in Fig. 3c), where magnetic moments point in the same direction. Here, the ice-rule dominates, as the three-nanomagnet vertices order such that they satisfy the constraints given by the ice-rule, while still attempting to minimize the J_2 and J_3 interactions as much as possible.

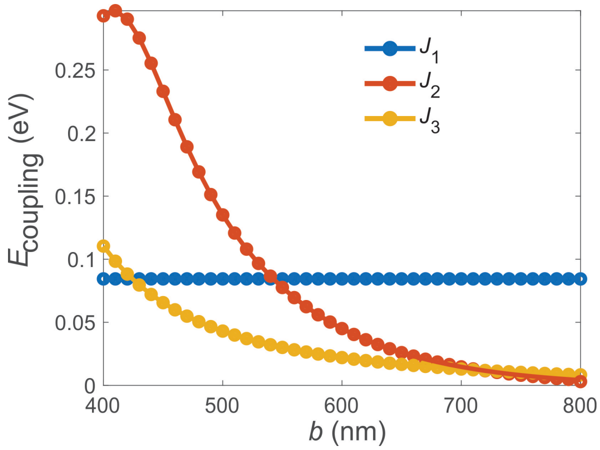

FIG. 2. Competing interaction strengths J_1, J_2 and J_3 plotted as a function of lattice parameter b. Most relevant to the competition between short-range ordered ice-rule domination and long-range ordered vortex formations is the equalization of J_1 and J_2 around b = 542 nm where the dominant coupling changes from J_2 to J_1.

The real-space observations are quantitatively evaluated by extracting nearest-neighbour correlation measures, as has been done for other artificial spin ice systems[2,3,5,21]. A correlation measure C between moments such as α and β (see Fig. 1b), labeled as $C_{\alpha\beta}$, is given a value +1, if the inner product of these moments is positive and a value −1, if their inner product is negative. The average is then calculated for the entire spin configuration. The correlation measures plotted as a function of b in Fig. 3e, perfectly reflect the aforementioned visual observations. At b = 500 nm, the long-range vortex-dominated order is reflected by the correlation measures being close to the maximum values ±1 (see Fig. 3e). Interestingly, already at b = 545 nm, $C_{\alpha\beta}$

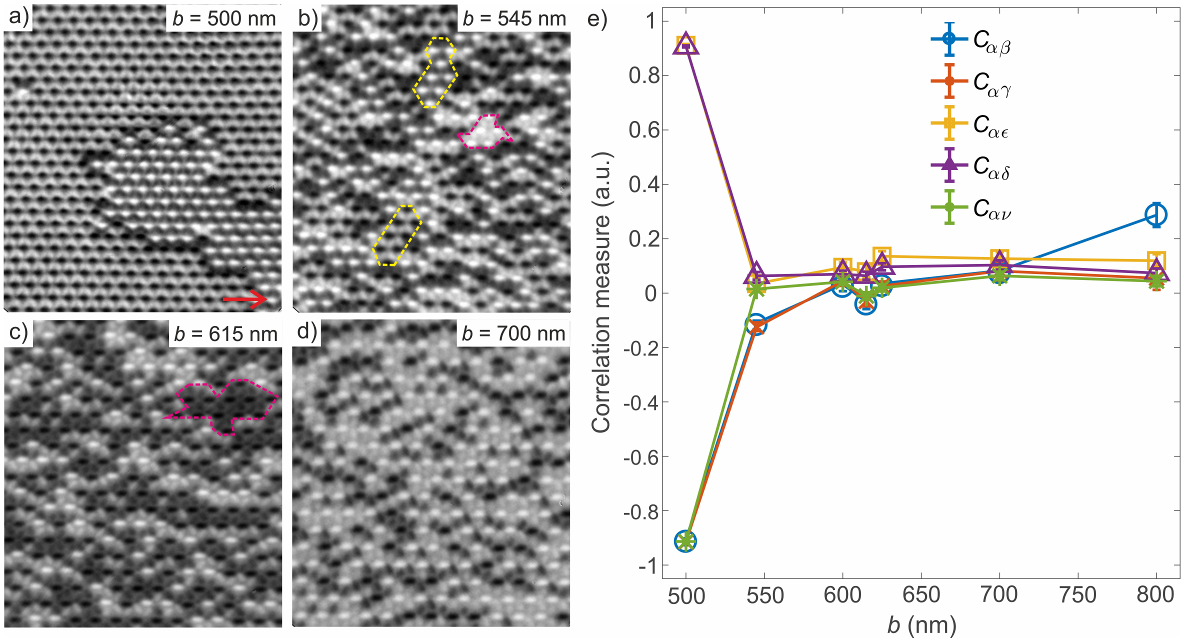

FIG. 3. (a)-(d) XMCD images (recorded at 90 K,) of frozen low-energy states achieved after thermal annealing on trimerized triangular lattices with lattice parameter (a) $b = 500$ nm, (b) $b = 545$ nm, (c) $b = 615$ nm and (d) $d = 700$ nm. The red arrow in (a) indicates the incoming X-ray direction. Magnetic moments pointing towards the X-rays will appear dark, while moments pointing in the opposite direction will appear bright. The yellow dashed frames in (b) highlight clusters of vortex-dominated configurations, while the magenta dashed frames in (b) and (c) highlight ferromagnetic-type clusters, where all magnetic moments point into one direction. (d) Spin correlation measures extracted from low-energy configurations plotted as a function of lattice parameter b. The error bars are standard deviations resulting from 10-15 annealed configurations at each value of b.

and $C_{\alpha\gamma}$ reduce to values between 0 and -0.1, while all other correlations drastically drop to positive values between 0 and 0.1 (see Fig. 3e). From that point onwards, all correlation measures seem to fluctuate between -0.1 and 0.1, as b increases, while $C_{\alpha\beta}$ consistently increases towards values close to 0.333 (see Fig. 3e). This particular value of 0.333 represents a strict ice-rule obedience[3,14] and indicates that the system is indeed moving towards an ice-rule dominated order at higher values of the lattice parameter b. The persistent small positive values of other correlation measures, for example $C_{\alpha\epsilon}$ (see Fig. 3e), indicates that long-range ferromagnetic-type ordering (domains of moments pointing in the same direction) is preferred. We infer that this is a direct consequence of the long-range nature of dipolar interactions between the patterned nanomagnetic vertices. In particular, interaction J_3, despite being the weakest of all three relevant nearest-neighbor interactions, supports such ferromagnetic ordering patterns and maintains ice-rule obedience. In other words, the long-range ferromagnetic order maintains satisfaction to both J_1 and J_3, making it the preferred ordering pattern with increasing b. It influences $C_{\alpha\epsilon}$ to remain weakly positive even at high b values and hinders the establishment of a purely short-range ordered phase dominated by strict ice-rule adherence with no long-range order.

While an ice-rule dominated order can theoretically support the formation of clockwise and anti-clockwise vortices at around 66% of all triangles (see Fig. 1f), this state is never experimentally observed. Instead, the system appears to transition from a vortex-driven phase for lattices with $b = 500$ nm to ferromagnetic states with ice-rule obedience and a vortex population of around 25% (see Fig. 4), at higher lattice spacings. This vortex population matches the statistical probability of randomly observing vortex states within a nanomagnet triangle (see inset in Fig. 4). When competing interactions J_1 and J_2 are equalized around $b = 545$ nm, 34% of the triangles still form a vortex states. From all these observations, it is obvious that the ferromagnetic ordering (pushed by J_3) strongly competes and limits the formation of vortices.

B. Temperature-dependent thermal fluctuations

As a next step, we turn our focus to temperature-dependent observations of thermal fluctuations in the dipolar trimerized triangular lattice (see example in the supplementary movie[52]). For comparison, we performed these measurements on two structures, the first having a lattice parameter $b = 545$ nm (close to the critical value of 542 nm) and the second with $b = 625$ nm. The structure with $b = 545$ nm had a blocking temperature $T_B = 142$ K, and we conducted our temperature-dependent observa-

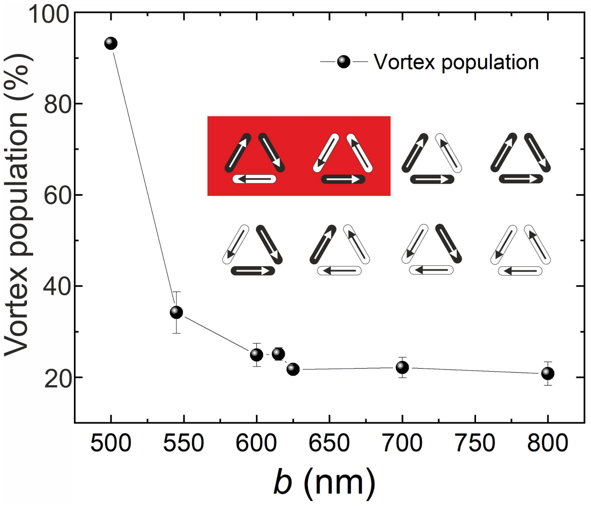

FIG. 4. Experimentally observed clockwise and anti-clockwise vortex populations plotted as a function of lattice parameter b. The inset highlights that two out of eight (25%) triangles form such vortex states, on purely statistical basis.

tions up to a temperature of 205 K. At six different temperatures between 142 K and 205 K, we recorded XMCD image sequences containing 70-100 images at each temperature. Magnetic configurations recorded within these image sequences allows us to extract temperature-dependent magnetic structure factors[13,19,21] (see Fig. 5a and Fig. 5b). The same type of experiment was performed on a structure with $b = 625$ nm between its blocking temperature $T_B = 170$ K and the highest temperature $T = 217$ K, ,above which thermal fluctuations become too fast for XMCD imaging. Again, temperature-dependent magnetic structure factors are extracted (see Fig. 5c and Fig. 5d). Visually, from real-space observations, we see that the system transitions from a vortex-dominated long-range ordered ground state to a more ferromagnetic-type ordering. The lattice with $b = 545$ nm, where competing interactions are equalized (see Fig. 2), exhibits a highly diffuse scattering pattern throughout the entire temperature range (see Fig. 5a and Fig. 5b), which reflects the high degree of frustration-induced disorder in this system. The $b = 625$ nm lattice shows sharp peaks embedded in slightly diffusive backgrounds in its magnetic structure factors (see Fig. 5c and Fig. 5d). In order to quantitatively understand these patterns, it is useful to look at magnetic structure factors calculated for a fully ordered vortex state (see Fig. 5e) and a multi-domain ferromagnetic state (see Fig. 5f). Doing so, we see that the peak positions $q =$ (0,2.3) best reflects ferromagnetic order. Looking at the temperature dependence of intensities at this peak position, we see that ferromagnetic order weakens for the $b = 545$ nm lattice (see Fig. 5g). In contrast to that, the (0,2.3) peak intensities for the $b = 625$ nm structure first decrease when going from 170 K to 190 K, before rapidly rising when heating towards 220 K (see Fig. 5h). In general, we see sharp peaks emerging in the magnetic structure factor that coincide with both ferromagnetic and vortex ordering, as the sample is heated (see Fig. 5c and Fig. 5d). A possible scenario that might explain this temperature dependence is that the $b = 625$ nm structure might be trapped in a local minimum upon cooling from room temperature, which is then overcome upon heating, as the system is allowed to explore more configurations and equilibrate in a phase that seems to combine features of a multi-domain long-range ferromagnetic order coinciding with clockwise and anti-clockwise vortices which occupy $21 - 25\%$ of all triangles.

IV. SUMMARY AND OUTLOOK

In summary, the trimerized triangular lattice is an interesting artificial frustrated spin system, which allows the combination of features from highly frustrated artificial kagome spin ice[3,7] and artificial triangular spin ice[45]. It exhibits various competing interactions, which can be directly controlled by the lattice parameter b. Tuning of the strengths of the interactions allows it to transition from a long-range ordered ground state dominated by clockwise- and anti-clockwise vortices, through a highly disordered state, when competing interactions are equalized, to a phase manifested by an increasing ice-rule obedience and a preference for ferromagnetic-type moment alignments. The variety of ordering preferences as interactions J_1 and J_2 are varied and equalized pose interesting questions, regarding its ground state and potential phase transitions at lower or higher temperatures, which can be either addressed via simulations[41,53,54] or experimentally, if structures with lowered blocking temperatures can be generated[55]. Newly emerging coherent X-ray scattering techniques[56] appear to be the best method for shedding light into these open questions. Three-nanomagnet trimers and kagome-based artificial spin ice systems also pose an intriguing case for studies on spin dynamics[31,57,58] and the dipolar trimerized triangular lattice will be an interesting addition to those investigations.

V. ACKNOWLEDGEMENTS

This work was supported by the Swiss National Science Foundation (Project No. 200020_172774 and Project No. 174306). S.v.D. acknowledges support from the Academy of Finland (Project No. 316857). M.S. acknowledges the support of the Center for Nonlinear Studies and Theory Division at Los Alamos, LA-UR-21-23310. Part of this work was performed at the SIM beamline of the Swiss Light Source (SLS), Paul Scherrer Institute, Villigen, Switzerland. The samples were fabricated at the Molecular Foundry, Lawrence Berkeley National Laboratory, Berkeley, USA. The Molecular Foundry is supported by the Office of Science, Office of

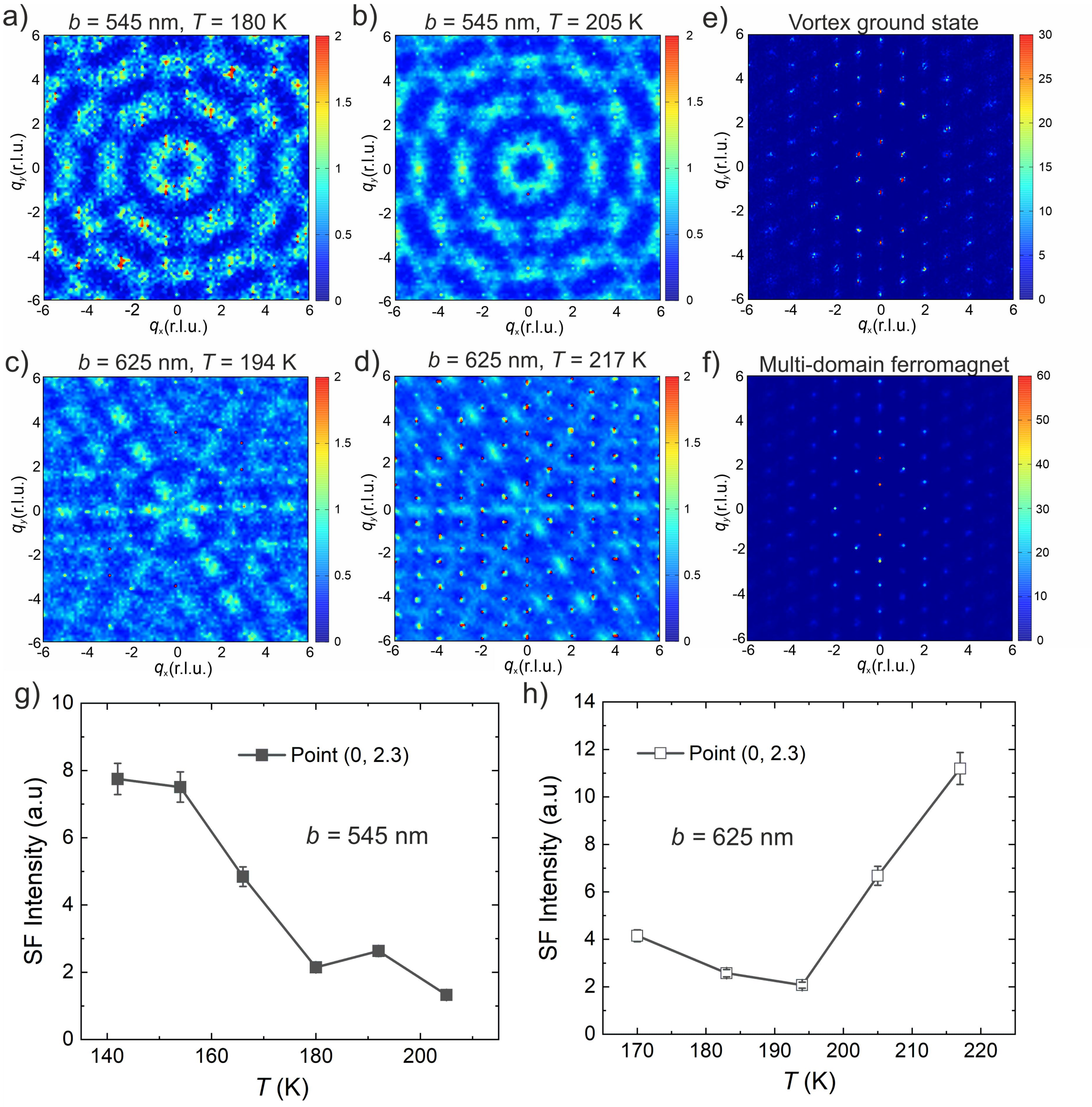

FIG. 5. (a)-(b) Magnetic structure factors for the $b = 545$ nm sample at (a) $T = 180$ K and (b) $T = 205$ K. The x and y axis are plotted in reciprocal lattice units (r.l.u.) using a unit cell of length of $a + b$. (c)-(d) Magnetic structure factors for the sample with $b = 625$ nm recorded at (c) $T = 194$ K and (d) $T = 217$ K. (e) Calculated magnetic structure factor of a long-range ordered state consisting of clockwise and anti-clockwise vortices. (f) Calculated magnetic structure for a multi-domain ferromagnetic phase within a trimerized triangular lattice. (g) Temperature-dependence of structure factor intensities for the $b = 545$ nm structure, at $q = (0,2.3)$ in q-space, which reflects the evolution of ferromagnetic order as a function of temperature. (h) Same temperature dependence for the $b = 625$ nm sample. The error bars in (g) and (h) result from standard deviations from sequences containing 70-100 images at each temperature.

Basic Energy Sciences, of the U.S. Department of Energy under Contract No. DE-AC02-05CH11231.

---

[*] alan.farhan@gmx.net

[1] S. H. Skjærvø, C. H. Marrows, R. L. Stamps, and L. J. Heyderman, Nature Reviews Physics **2**, 13 (2020).

[2] R. F. Wang, C. Nisoli, R. S. Freitas, J. Li, W. McConville, B. J. Cooley, M. S. Lund, N. Samarth, C. Leighton, V. H. Crespi, and P. Schiffer, Nature **439**, 303 (2006).

[3] Y. Qi, T. Brintlinger, and J. Cumings, Physical Review B **77**, 094418 (2008).

[4] S. Ladak, D. E. Read, G. K. Perkins, L. F. Cohen, and W. R. Branford, Nature Physics **6**, 359 (2010).

[5] N. Rougemaille, F. Montaigne, B. Canals, A. Duluard, D. Lacour, M. Hehn, R. Belkhou, O. Fruchart, S. El Moussaoui, A. Bendounan, and F. Maccherozzi, Physical Review Letter **106**, 057209 (2011).

[6] J. P. Morgan, A. Stein, S. Langridge, and C. H. Marrows, Nature Physics **7**, 75 (2011).

[7] A. Farhan, P. M. Derlet, A. Kleibert, A. Balan, R. V. Chopdekar, M. Wyss, L. Anghinolfi, F. Nolting, and L. J. Heyderman, Nature Physics **9**, 375 (2013).

[8] I. Gilbert, G.-W. Chern, S. Zhang, L. O'Brien, B. Fore, C. Nisoli, and P. Schiffer, Nature Physics **10**, 670 (2014).

[9] Y. Li, G. W. Paterson, G. M. Macauley, F. S. Nascimento, C. Ferguson, S. A. Morley, M. C. Rosamond, E. H. Linfield, D. A. MacLaren, R. Macêdo, C. H. Marrows, S. McVitie, and R. L. Stamps, ACS Nano **13**, 2213 (2018).

[10] I. Gilbert, Y. Lao, I. Carrasquillo, L. O'Brien, J. D. Watts, M. Manno, C. Leighton, A. Scholl, C. Nisoli, and P. Schiffer, Nature Physics **12**, 162 (2016).

[11] A. Farhan, A. Scholl, C. F. Petersen, L. Anghinolfi, C. Wuth, S. Dhuey, R. V. Chopdekar, P. Mellado, M. J. Alava, and Sebastiaan van Dijken, Nature Communications **7**, 12635 (2016).

[12] J. Drisko, T. Marsh, and J. Cumings, Nature Communications **8**, 14009 (2017).

[13] Y. Perrin, B. Canals, N. Rougemaille, Nature **540**, 410 (2016).

[14] A. Farhan, P. M. Derlet, L. Anghinolfi, A. Kleibert, and L. J. Heyderman, Physical Review B **96**, 064409 (2017).

[15] C. F. Petersen, A. Farhan, S. Dhuey, Z. Chen, M. J. Alava, A. Scholl, and S. van Dijken, Applied Physics Letters **112**, 092403 (2018).

[16] D. Shi, Z. Budrikis, A. Stein, S. A. Morley, P. D. Olmsted, G. Burnell, and C. H. Marrows, Nature Physics **14**, 309 (2018).

[17] M. Saccone, K. Hofhuis, Y.-L. Huang, S. Dhuey, Z. Chen, A. Scholl, R. V. Chopdekar, S. van Dijken, and A. Farhan, Physical Review Materials **3**, 104402 (2019).

[18] D. Louis, D. Lacour, M. Hehn, V. Lomakin, T. Hauet, and F. Montaigne, Nature Materials **17**, 1076 (2018).

[19] A. Farhan, M. Saccone, C. F. Petersen, S. Dhuey, R. V. Chopdekar, Y.-L. Huang, N. Kent, Z. Chen, M. J. Alava, T. Lippert, A. Scholl, S. van Dijken, Science Advances **5**, eaav6380 (2019).

[20] A. May, M. Hunt, A. Van Den Berg, A. Hejazi, and S. Ladak, Communications Physics **2**, 13 (2019).

[21] A. Farhan, M. Saccone, C. F. Petersen, S. Dhuey, K. Hofhuis, R. Mansell, R. V. Chopdekar, A. Scholl, T. Lippert, and S. van Dijken, Physical Review Letters **125**, 267203 (2020).

[22] M. J. Harris, S. T. Bramwell, D. F. McMorrow, T. Zeiske and K. W. Godfrey, Physical Review Letter **79**, 2554 (1997).

[23] N. Rougemaille, and B. Canals, Eur. Phys. J. B **92**, 62 (2019).

[24] A. Farhan, P. M. Derlet, A. Kleibert, A. Balan, R. V. Chopdekar, M. Wyss, J. Perron, A. Scholl, F. Nolting, and L. J. Heyderman, Physical Review Letters **111**, 057204 (2013).

[25] V. Kapaklis, U. B. Arnalds, A. Farhan, R. V. Chopdekar, A. Balan, A. Scholl, L. J. Heyderman, and Björgvin Hjörvarsson, Nature Nanotechnology **9**, 514 (2014).

[26] M. Saccone, K. Hofhuis, D. Bracher, A. Kleibert, S. van Dijken, and A. Farhan, Nanoscale **12**, 189 (2020).

[27] M. Saccone, A. Scholl, S. Velten, S. Dhuey, K. Hofhuis, C. Wuth, Y.-L. Huang, Z. Chen, R. V. Chopdekar, and A. Farhan, Physical Review B **99**, 224403 (2019).

[28] J. Sklenar, Y. Lao, A. Albrecht, J. D. Watts, C. Nisoli, G.-W. Chern, and P. Schiffer, Nature Physics **15**, 191 (2019).

[29] S. Gliga, A. Kákay, R. Hertel, and O. G. Heinonen, Physical Review Letters **110**, 117205 (2013).

[30] M. B. Jungfleisch, W. Zhang, E. Iacocca, J. Sklenar, J. Ding, W. Jiang, S. Zhang, J. E. Pearson, V. Novosad, J. B. Ketterson, O. Heinonen, and A. Hoffmann, Physical Review B **93**, 100401(R) (2016).

[31] V. S. Bhat, F. Heimbach, I. Stasinopoulos, and D. Grundler, Physical Review B **93**, 140401(R) (2016).

[32] A. Talapatra, N. Singh, and A. O. Adeyeye, Physical Review Applied **13**, 014034 (2020).

[33] D. M. Arroo, J. C. Gartside, and W. R. Branford, Physical Review B **100**, 214425 (2019).

[34] V. M. Parakkat, K. Xie, and K. M. Krishnan, Physical Review B **99**, 054429 (2019).

[35] V. M. Parakkat, G. M. Macauley, R. L. Stamps, and K. M. Krishnan, Physical Review Letters **126**, 017203 (2021).

[36] A. Ortiz-Ambrez, P. Tierno, Nature Communications **7**, 10575 (2016).

[37] A. Libál, C. Nisoli, C. J. O. Reichhardt, C. Reichhardt, Physical Review Letters **120**, 027204 (2018).

[38] D.-Y. Lee, and P. Tierno, Physical Review Materials **2**, 112601(R) (2018).

[39] A. Libál, D.-Y. Lee, A. Ortiz-Ambriz, C. Reichhardt, C. J. O. Reichhardt, P. Tierno, and C. Nisoli, Nature Communications **9**, 4146 (2018).

[40] P. Mellado, A. Concha, and L. Mahadevan, Physical Review Letters **109**, 257203 (2012).

[41] G. Möller and R. Moessner, Physical Review B **80**, 140409(R) (2009).

[42] I. A. Chioar, B. Canals, D. Lacour, M. Hehn, B. Santos Burgos, T. O. Menteş, A. Locatelli, F. Montaigne, and N. Rougemaille, Physical Review B **90**, 220407(R) (2014).

[43] Y. Shevchenko, A. Makarov, K. Nefedev, Physics Letters A **381**, 428 (2017).

[44] G.-W. Chern, P. Mellado, Europhysics Letters **114**, 37004 (2016).

[45] L. A. S. Mól, A. R. Pereira, and W. A. Moura-Melo, Physical Review B **85**, 184410 (2012).

[46] J. H. Rodrigues, L. A. S. Mól, W. A. Moura-Melo, and A. R. Pereira, Applied Physics Letters **103**, 092403 (2013).

[47] J. M. Porro, A. Bedoya-Pinto, A. Berger, and P. Vavassori, New Journal of Physics **15**, 055012 (2013).

[48] L. Le Guyader, A. Kleibert, A. Fraile Rodríguez, S. El Moussaoui, A. Balan, M. Buzzi, J. Raabe, and F. Nolting, J. Elec. Spec. Rel. Phenom. **185**, 371 (2012).

[49] J. Stöhr Y. Wu, B. D. Hermsmeier, M. G. Samant, G. R. Harp, S. Koranda, D. Dunham, and B. P. Tonner, Science **259**, 658 (1993).

[50] A. Vansteenkiste, J. Leliaert, M. Dvornik, M. Helsen, F. Garcia-Sanchez, and B. Van Waeyenberge, AIP Advances **4**, 107133 (2014).

[51] A. Farhan, C. F. Petersen, S. Dhuey, L. Anghinolfi, Q.-H. Qin, M. Saccone, S. Velten, C. Wuth, S. Gliga, P. Mellado, M. J. Alava, A. Scholl, S. van Dijken, Nature Communications **8**, 995 (2017).

[52] See Supplemental Material at [URL will be inserted by publisher] [Supplementary Movie 1: XMCD sequence showing thermal fluctuations in a dipolar trimer lattice with $b = 175$ nm at $T = 183$ K.].

[53] G.-W. Chern, P. Mellado, and O. Tchernyshyov, Physical Review Letters **106**, 207202 (2011).

[54] K. Makarova, V. Strongin, I. Titovets, A. Syrov, I. Zinchenko, V. Samoylov, K. Hofhuis, M. Saccone, A. Makarov, A. Farhan, and K. Nefedev, Physical Review E **103**, 042129 (2021).

[55] K. Hofhuis, A. Hrabec, H. Arava, N. Leo, Y.-L. Huang, R. V. Chopdekar, S. Parchenko, A. Kleibert, S. Koraltan, C. Abert, C. Vogler, D. Suess, P. M. Derlet, and L. J. Heyderman, Physical Review B **102**, 180405(R) (2020).

[56] X. M. Chen, B. Farmer, J. S. Woods, S. Dhuey, W. Hu, C. Mazzoli, S.B. Wilkins, R. V. Chopdekar, A. Scholl, I. K. Robinson, L. E. De Long, S. Roy, J.T. Hastings Physical Review Letters **123**, 197202 (2019).

[57] W. Bang, F. Montoncello, M. B. Jungfleisch, A. Hoffmann, L. Giovannini, and J. B. Ketterson, Physical Review B **99**, 014415 (2019).

[58] M. Taghipour Kaffash, W. Bang, S. Lendinez, A. Hoffmann, J. B. Ketterson, and M. B. Jungfleisch, Physical Review B **101**, 174424 (2020).